CHEMISTRY
A EUROPEAN JOURNAL

DOI: 10.1002/chem.200500649

VIP

TiO_2 Nanoparticles in Mesoporous TUD-1: Synthesis, Characterization and Photocatalytic Performance in Propane Oxidation

Mohamed S. Hamdy,[a] Otto Berg,[b] Jacobus C. Jansen,[c] Thomas Maschmeyer,[d] Jacob A. Moulijn,[a] and Guido Mul*[a]

Abstract: A series of TiO_2-TUD-1 samples was synthesized with a variable Ti loading in the range Si/Ti = 100, 20, 2.5, and 1.6, by using a one-pot surfactant-free procedure. The materials obtained were characterized by elemental analysis; X-ray diffraction (XRD); N_2 sorption measurements; high-resolution TEM (HR-TEM); ^{29}Si NMR, UV-visible and Raman spectroscopy. As a function of increasing metal loading either isolated Ti atoms, or (above a Ti loading of ~2.5 wt-%) combinations of isolated Ti atoms and anatase (TiO_2) nanoparticles were obtained; both were incorporated in the highly porous siliceous matrix. The photocatalytic performance of these materials was tested by studying the propane oxidation process following irradiation at $\lambda =$ 365 nm, selectively activating the anatase nanoparticles. In comparison to commercial anatase powder, TiO_2 nanoparticles in TUD-1 showed high photochemical selectivity towards acetone, the sample with a Si/Ti ratio of 1.6 being the most selective. Size and confinement effects are consistent with the difference in performance of the TUD-1 materials and TiO_2, limiting the number of electron transfers available for each propane molecule.

Keywords: anatase · mesoporous materials · nanoparticles · oxidation · photocatalysis

Introduction

The development of a selective direct route for partial oxidation of propane is of major industrial importance, as it would allow for an efficient use of this ubiquitous feedstock in important large-scale applications, such as polymer synthesis. Regarding the development of catalysts to effect such reactions, many of the reported approaches rely on thermal activation at elevated temperature. Photocatalysis at ambient temperature is an alternative that could, in principle, be highly selective. Photooxidation of light alkanes and alkenes over titania[1–5] and silica-supported titania with UV irradiation has indeed been reported.[6–8] Photocatalytic, UV-driven oxidation of light alkanes and alkenes over titania[1–8] is largely nonselective, while over silica-supported titania reasonable selectivities in, for example, propane oxidation to acetone have been reported.[6–8] It should be mentioned that in these studies usually a variety of wavelengths, emitted by for example, mercury and deuterium lamps, was used to activate the catalysts.

The high activity and low selectivity of bulk titania as a photocatalyst has been explained by a relatively high concentration of holes (h^+), which are associated with surface O atoms. These holes are highly mobile, thus allowing multiple electron transfers, which are required for complete oxidation of organic molecules to CO_2 and water.[8] When a semiconductor is prepared in the form of sufficiently small particles or isolated sites (which is possible on amorphous high surface-area supports (SiO_2) or in micro- or mesoporous materials), the insulating nature of the support is proposed to limit the transport of the holes and, thus, the number of electron transfers that are accessible to each adsorbed organic molecule in an oxidation process.[8] When

[a] Dr. M. S. Hamdy, Prof. Dr. J. A. Moulijn, Dr. G. Mul
Reactor and Catalysis Engineering(R&CE)
DelftChemTech, Technische Universiteit Delft
Julianalaan 136, 2628 BL, Delft (The Netherlands)
Fax: (+31) 15-278-5006
E-mail: g.mul@tnw.tudelft.nl

[b] Dr. O. Berg
Leiden Institute of Chemistry, Leiden University
Einsteinweg 55, P.O Box 9502
2300 RA Leiden (The Netherlands)

[c] Dr. J. C. Jansen
Ceramic Membrane Centre (The Pore)
Technische Universiteit Delft, Julianalaan 136
2628 BL, Delft (The Netherlands)

[d] Prof. Dr. T. Maschmeyer
Laboratory of Advanced Catalysis for Sustainability
School of Chemistry, The University of Sydney
NSW 2006 (Australia)

micro- or mesoporous materials are used, confinement of the particles is expected to further enhance selectivity.

In the present study incorporation of TiO_2 in a new mesoporous material developed at the Delft University of Technology (TUD-1) was evaluated for the selective light-activated oxidation of propane to acetone. TUD-1 is a form of mesoporous amorphous silica with a 3D spongelike structure.[9] The functionalization of TUD-1 with a low loading of titanium (denoted Ti-TUD-1) has been reported previously[10] and it showed high activity in cyclohexene epoxidation. In the present study, it will be shown that one of the advantages of using TUD-1 as a support is that a high loading of titanium can be achieved, while maintaining a high dispersion of TiO_2 in the form of nanoparticles. These nanoparticles have a narrow size distribution, due to the growth conditions within the aggregates of a templated sol–gel synthesis. A further consequence is that these nanoparticles are located on accessible surfaces of the mesopore. In this paper, we report an extensive characterization of the TiO_2 nanoparticles embedded in a TUD-1 mesoporous silica matrix. It will also be shown that nanoparticle-containing TiO_2-TUD-1 can be more selective in the photooxidation of propane to acetone than commercially available microcrystalline anatase; this result is based on activity evaluation using IR spectroscopy. In contrast to previously reported studies on the use of SiO_2-supported TiO_2 catalysts, in which multiple wavelength excitation was applied, irradiation was performed in this work at a distinct wavelength of $\lambda = 365$ nm. Implications for the structure/activity correlation of the nanoparticles are discussed.

Results and Discussion

TiO_2-TUD-1—a new mesoporous material: All TiO_2-TUD-1 samples (nomenclature in Table 1) were prepared at room temperature by using triethanolamine (TEA) as a bifunctional template, which acts as a mesopore-directing agent and as a complexing ligand[11] for titanium-active sites on the mesoporous wall. The Si/Ti ratio in the synthesis gel and in the calcined product are plotted in Figure 1, the latter being determined by instrumental neutron activation analysis (INAA), a technique for elemental analysis. The Si/Ti ratio in the final product after calcination is close to that present in the synthesis gel, which indicates that most titanium cations are incorporated in the final solid product.

Table 1. Elemental analysis and the N_2 sorption measurements of TiO_2-TUD-1.

Sample	Si/Ti ratio in synthesis mixture	Si/Ti ratio after calcination	S_{BET}[a] [$m^2 g^{-1}$]	V_{meso}[b] [$cm^3 g^{-1}$]	D_{meso}[c] [nm]	Color
Ti-1	100	105	628	1.1	9.1	white
Ti-20	5	4.6	741	0.5	3.6	white
Ti-40	2.5	2.3	570	0.36	3.5	white
Ti-60	1.6	1.4	516	0.28	2	white

[a] Specific surface area. [b] Mesopore volume. [c] Mesopore diameter.

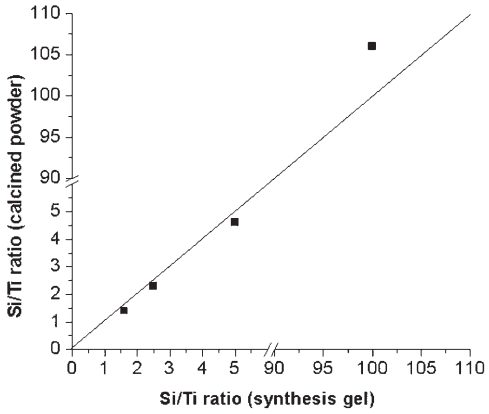

Figure 1. Elemental analysis in terms of Si/Ti molar ratio in the synthesis gel versus the Si/Ti molar ratio in the final products.

Moreover, this demonstrates that the outcome of the synthesis is highly predictable.

^{29}Si NMR spectroscopy is a well-established tool for the characterization of crystalline silicate minerals, allowing for the detection of heteroatoms incorporated in the framework;[12] in principle this should also be possible for mesoporous amorphous materials. The ^{29}Si magic angle spinning NMR (MAS NMR) spectrum of calcined siliceous TUD-1 is shown in Figure 2, together with sketches of the Si-bearing structures responsible.[14] The principal peak, centered at $\delta = -110$ ppm, is usually labeled Q_4 and assigned to $Si(-O-)_4$ units that do not involve silanol (SiOH). The shoulder at $\delta = -102$ ppm (Q_3) is assigned to silicon nuclei with a single silanol group, $Si(OH)(-O-)_3$. A signal at $\delta = -90$ ppm (Q_2), characteristic of $Si(OH)_2(-O-)_2$, is very weak in TUD-1. Also shown in Figure 2 is the spectrum of TiO_2-TUD-1, normalized to the same peak intensity. As TiO_2-TUD-1 contains fewer Si nuclei, its signal-to-noise ratio is lower. In the region of Q_4, Q_3, and Q_2 the observed band shapes are identical. The only deviation that might be assigned to the heteroatomic structure $Si-O-Ti(-O-)_3$ is a weak shoulder in the region $\delta = -122$ to -132 ppm. In general, however,

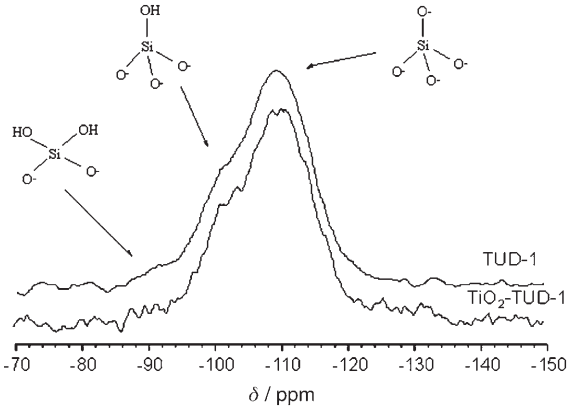

Figure 2. ^{29}Si NMR spectra for TUD-1 (upper) and TiO_2-TUD-1 (lower, offset).

most of the silica in TiO_2-TUD-1 is chemically similar to that in pure TUD-1.

Figure 3 shows powder X-ray diffraction (XRD) patterns of various samples of TiO_2-TUD-1. Different Ti loadings are denoted by a relative weight percent of Ti, with the corresponding Si/Ti ratio reported in Table 1. All samples show a single intense peak at 1–2.5° 2θ, which corresponds to a short-range correlation of nuclear density at a distance of 45–47 Å. The peak is instrument-limited on the small-angle side, but with increasing Ti content it weakens, broadens, and shifts to larger angles. This implies that the short-range order is increasingly disrupted, and that the remaining structures are smaller and more heterogeneous. This indicates that TiO_2-TUD-1 is a noncrystalline, mesostructured material. The intensity of the peak decreases with increasing Ti loading as a result of the influence of titania particles on the integrity of the mesoporous structure. Crystalline TiO_2 (anatase or rutile) could not be detected with XRD.

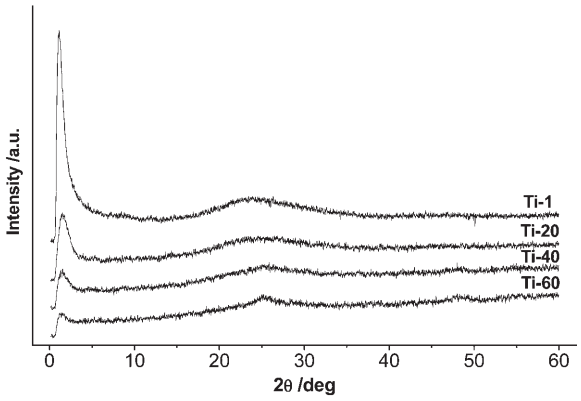

Figure 3. XRD patterns of TiO_2-TUD-1 samples.

Figure 4 shows N_2 sorption isotherms of the TiO_2-TUD-1 samples. All TiO_2-TUD-1 samples show type IV adsorption isotherms, indicating their mesostructured character[15] with narrow pore-size distribution. One can distinguish two characteristic types of hysteresis loops. In the first case, (i.e., Ti-1) the loop is relatively narrow, the adsorption and desorption branches being almost vertical and nearly parallel. This indicates that the isotherm is governed by delayed capillary condensation, with uniformly sized pores filling and emptying in a narrow pressure range. At higher Ti loading (Ti-20, Ti-40, and Ti-60) the hysteresis loop becomes broad, the desorption branch being steeper than that of the adsorption branch at relative pressures of about 0.4–0.5. This feature is characteristic of mass-transfer-limited filling and emptying of nonuniform pores. The presence of TiO_2 nanoparticles clearly affects the internal structure and connectivity of TUD-1.

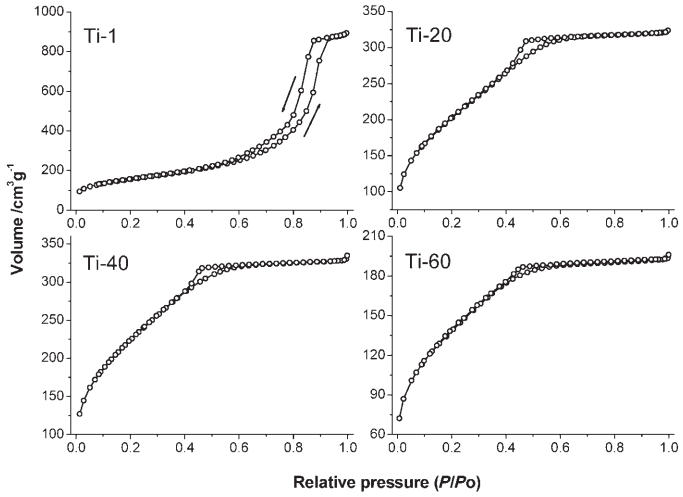

Figure 4. The N_2 adsorption isotherms for different TiO_2-TUD-1 samples.

In Table 1 porosity measurements of the TiO_2-TUD-1 samples (calculated from the adsorption branch of the N_2 adsorption–desorption isotherms using the Barrett–Joyner–Halenda formula) are summarized: the surface area of the samples ranges from 500 to 750 m^2g^{-1}, the mesopore volume decreases with Ti loading from 1.1 to 0.28 cm^3g^{-1}, and the mesopore diameter from 9.1 to 2 nm. These trends are in agreement with those observed in the corresponding series of XRD patterns.

Figure 5 shows diffuse reflectance UV-visible spectra of different TiO_2-TUD-1 samples. All spectra contain an absorption band centered at 220 nm, which is attributed to the charge-transfer transition associated with isolated Ti^{4+} framework sites in tetrahedral coordination.[16] The other peak around 320–350 nm indicates the presence of polytitanium $(Ti–O–Ti)_n$ clusters.[17] The intensity of this peak increases with Ti loading, consistent with the formation of a crystalline TiO_2 phase in addition to the titanosilicate phase. This crystalline phase is nevertheless not apparent in the powder XRD patterns (above), indicating large Debye–Scherrer broadening consistent with their small size.

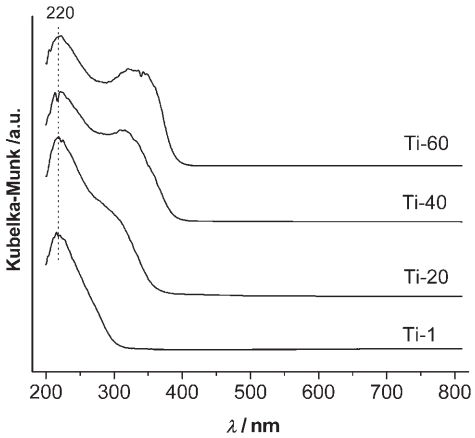

Figure 5. The UV-visible spectra for TiO_2-TUD-1 samples.

To clarify the distribution of crystalline titania within the various TiO_2-TUD-1 samples, a high-resolution transmission

electron microscopy (HR-TEM) study was performed. The images of Ti-1 (Figure 6) show only the spongelike 3D structure characteristic of TUD-1 mesoporous materials; this is a strong indication for the complete isolation of Ti atoms inside the framework. In contrast to highly ordered materials, like MCM-41, the apparent pore size is not directly proportional to that obtained from the nitrogen-sorption experiments. It appears significantly smaller, due to the superposition of many disordered pores within the focal depth of the microscope. In the images of Ti-20, Ti-40, and Ti-60 the spongelike mesoporous matrix is still apparent. More importantly, the diffraction fringes of TiO_2 nanocrystals are observed. These appear as evenly distributed, uniform inclusions, rather than bulky crystals or heterogeneous aggregates. The size of the nanoparticles is comparable to that of the pores in TUD-1. This suggests that nanoparticle growth is limited by the pore diameter, and therefore these particles nucleate and grow within existing pores of the matrix.

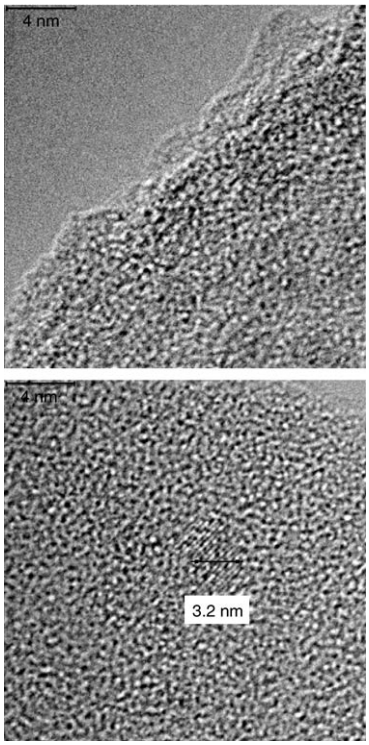

Figure 6. HR-TEM images for Ti-1 (top) and Ti-40 (bottom).

In Figure 7 a HR-TEM image of the Ti-40 sample is presented. The major *d*-spacings are indicated and for comparison those for anatase and rutile are also presented. The results suggest that the crystalline phase is anatase, although the d_{101} value deviates to some extent.[18] In Figure 8 the Raman spectra of dehydrated Ti-1 and Ti-60 samples are compared with those of anatase and rutile. Based on Raman spectra of the anatase and rutile reference materials, it can be inferred that these samples were not entirely single phase (rutile contained some anatase phase, and anatase some rutile phase). However, for phase identification of the TUD-1 catalysts these samples served their purpose. Ti-1 did not show any Raman resonance in the frequency range in which anatase and rutile peaks appeared; this is consistent with results from other characterization techniques. The Raman spectrum of Ti-60 matches that of anatase, demonstrating conclusively the presence of anatase as nanosize crystals in TiO_2-TUD-1.

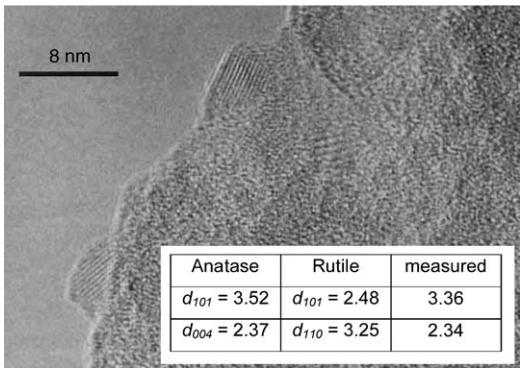

Figure 7. HR-TEM image of a Ti-40 sample. The inset gives the standard *d*-spacing of bulk rutile and anatase[18] compared with the measured values.

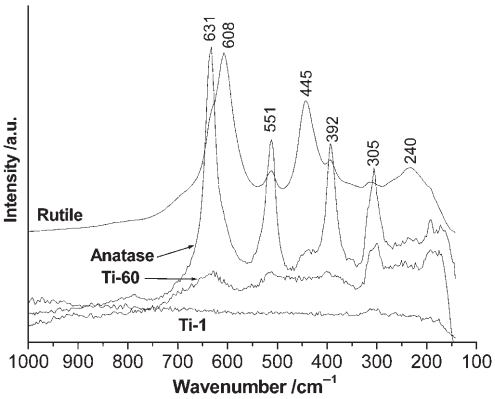

Figure 8. Raman spectra of TiO_2-TUD-1 compared with those of rutile and anatase.

The photocatalytic performance: The reaction of propane with molecular oxygen was used to evaluate the photocatalytic performance of TiO_2-TUD-1. Control experiments were carried out to demonstrate that oxygen gas, titanium loading, and near-UV irradiation were all necessary for the appearance of propane oxidation products. In these blank runs no products were observed in the IR spectrum after 100 minutes.

Exposure of the Ti-1 and Ti-20 samples to near-UV light in an atmosphere of propane and molecular oxygen had a minimal effect, consistent with the absence of electronic absorption at 365 nm (cf. Figure 5). Samples Ti-40 and Ti-60 absorb light at the excitation wavelength; this resonance was previously assigned to anatase inclusions. At the applied wavelength of 365 nm, the specific absorbance of Ti-60 is

greater by a factor of two (cf. Figure 5). Difference spectra before (a) and after irradiation (b) are shown in Figure 9 (10 mW cm^{-2} at 365 nm, 28 °C); this is typical for the Ti-60 catalyst. Because the background was recorded after dosing, the vibrational modes of propane are not apparent. The bands which appear during irradiation can be assigned as follows.

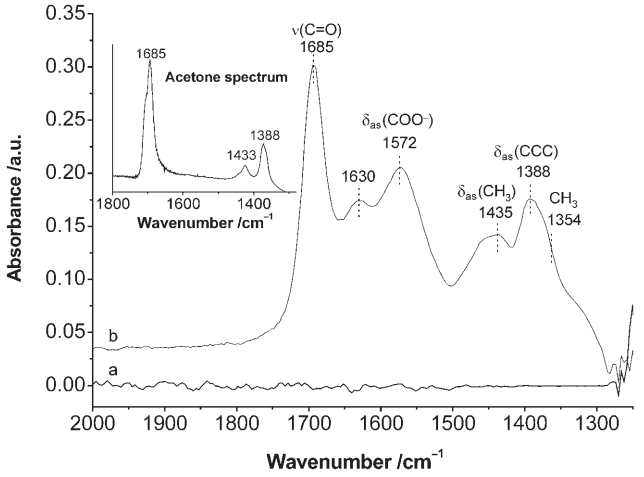

Figure 9. FTIR difference spectra of adsorbed species arising from propane oxidation over Ti-60 at a) zero time (dark) and b) after 100 minutes of photoexcitation. The inset shows a spectrum of acetone adsorbed directly from the gas phase.

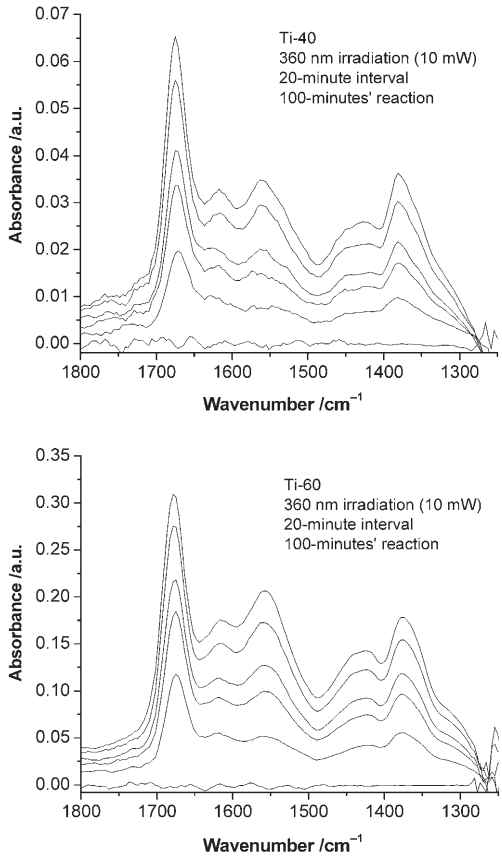

Figure 10. FTIR spectra of adsorped species arising from propane oxidation over Ti-40 (top) and Ti-60 (bottom).

The strongest band at 1685 cm^{-1} is characteristic of a carbonyl C=O stretching vibration. This, the C–C–C asymmetric stretching frequency at 1388 cm^{-1}, and the C–H bending mode at 1435 cm^{-1} are due to adsorbed acetone. For comparison, the spectrum of acetone adsorbed on TUD-1 is shown in the inset of Figure 9. The band at 1572 cm^{-1} and the shoulder of the band at 1435 cm^{-1} are attributed to asymmetric and symmetric stretching modes of the carboxyl group (COO^-), respectively. Acetate and/or formate species are the most probable carriers of this group and were reported to be formed by alkane and alkene oxidation over various transition metal oxides such as Cr_2O_3.[19] In fact, for formate the symmetric stretch overlaps with the 1388 cm^{-1} bending mode of adsorbed acetone, and the 1433 cm^{-1} absorption is typically correlated with the presence of acetate species .[19] For detailed information on surface oxidation of adsorbed C_3 species on TiO_2 to acetate and formate species the reader is referred to the work of Mul et al.[20] Finally, the peak at 1630 cm^{-1} can be assigned to the bending mode of water by comparing it with the spectra of reference systems (not shown). The development of the product spectra by photochemical activity of Ti-40 and Ti-60 is shown in Figure 10.

The product spectra can be quantified by deconvolution and integration of the component peaks, their areas being proportional to the number of molecules present. The constants of proportionality (integrated IR cross section) are known, allowing calculation of the activity and selectivity of the photochemical reaction. Any systematic errors due to the deconvolution procedure or uncertainty in the IR cross sections are internally consistent among the measurements given here, so comparisons are justified. The rate of total product formation, based on the photometric results, is plotted as a function of exposure time in Figure 11 for various TUD-1 samples. These quantities are specified per unit *external* surface area of the sample wafer (see Experimental

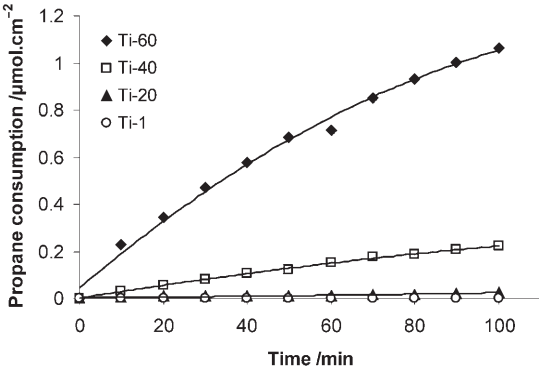

Figure 11. Propane consumption ([Acetone] + [Carboxylate/2] (μmol cm^{-2})) over different TiO_2-TUD-1 compositions.

Section); the corresponding internal surface available for adsorption is orders of magnitude greater.

Figure 11 shows that the activity of Ti-60 is significantly higher than that of Ti-40. As both samples absorb strongly at the excitation wavelength, and the transmitted power is negligible, most of the light is absorbed. The difference in specific optical absorption will affect the penetration depth of this radiation, but the IR photometry effectively sums over the entire sample thickness. With this in mind, the photon efficiency of the catalyst pellets can be estimated as follows: over the 100 minute reaction period a total of 1.1×10^{23} UV photons m^{-2} were incident on various samples, all of which were opaque at the excitation frequency. On Ti-60 this gives 1.1×10^{-6} mol cm^{-2} of products, or 1.8×10^{20} molecules m^{-2}. Therefore, the quantum yield of photochemical products is in the order of 0.002.

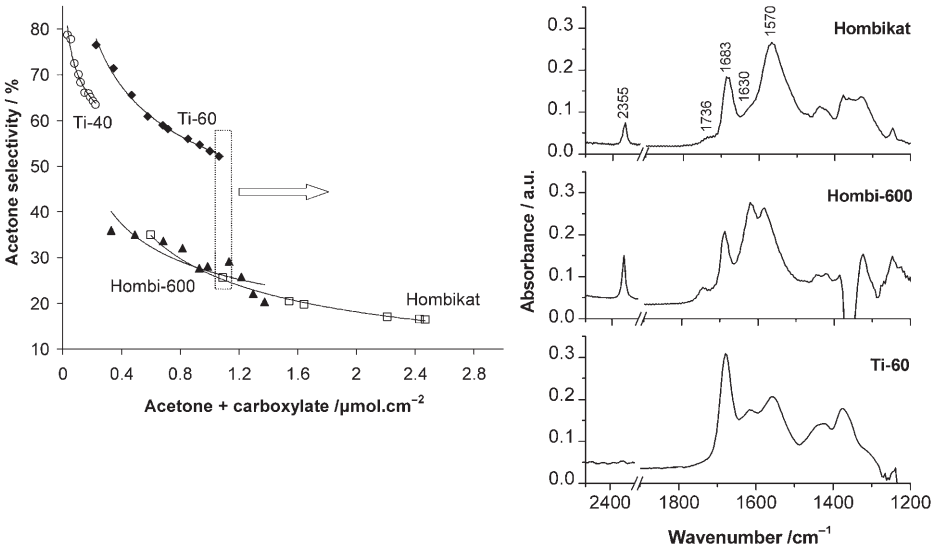

Figure 12. Left, surface acetone selectivity (%) as a function of total amount of acetone and carboxylates produced. Right, FTIR spectra of adsorbed species arising from propane oxidation over Ti-60 compared with pure bulk anatase (Hombikat and Hombi-600) after reaching the same amount of products, that is, ~1.1 µmol cm^{-2}.

The acetone production rate, as summarized in Table 2, is a factor of five higher in Ti-60 than in Ti-40. This suggests that the smaller particle size present in the Ti-60 sample (~2 nm) versus the Ti-40 sample (~3.5 nm), and the associated higher number of available Ti–O surface sites, contributes to the significantly higher performance of Ti–60. In addition to the rate of product formation, Table 2 also lists the selectivity. It shows that the Ti-60 sample is not only more active, but also more selective towards acetone in the oxidation of propane (vide infra).

Besides comparing the various TUD-1 samples in performance, it is particularly interesting to compare the performance of TiO_2-TUD-1 with pure bulk anatase TiO_2 (Hombikat) under the same reaction conditions. In Figure 12 the spectra of Ti-60 and two anatase samples at comparable conversion are shown. For the bulk anatase samples, the product spectra are dominated by carboxylate absorption frequencies. In contrast to any of the TiO_2-TUD-1 materials adsorbed CO_2 was also generated during the reaction (asymmetric stretch at 2355 cm^{-1}), as well as aldehyde species (C=O stretch at 1736 cm^{-1}). The formation of aldehydes has been reported previously by Yoshida and co-workers,[6,7] although the data are largely confusing and no explanation is given. The differences in product distribution between the two Hombikat samples are most likely the result of a different surface hydroxyl-group concentration and surface area and porosity of the samples, induced by the thermal pretreatment at 873 K. Pure anatase phases (Hombikat) clearly favor over-oxidation products, up to and including complete oxidation to H_2O and CO_2.

The selectivity to acetone as a function of total product formation is also given in Figure 12. Over the whole propane conversion range investigated, the TUD-1 samples are much more selective toward acetone than bulk anatase phases, while Ti-60 seems to be the most selective catalyst. The low selectivity for the anatase samples is in good agreement with literature data. Among others, Brigden et al.[4] and Haeger et al.[5] reported complete oxidation to CO_2 under conditions relevant for environmental pollution control applications, that is, with a large excess of O_2 of about 200 relative to the alkane and alkene concentrations. In fact, a similar O_2 over propane ratio of 140 was employed in the present study to prevent, as much as possible, a rapid deactivation of the catalysts.[4,5] Still, in Figure 11 some deactivitation of the Ti-60 catalyst can be observed, which is explained by the large amount of acetone and carboxylate accumulating on the catalyst surface. In view of the large oxygen excess, it is

Table 2. The activity measurements of propane oxidation over different TiO_2-TUD-1 samples.

Sample	Surface rate $\times10^3$ [µmol cm^{-2} min^{-1}]	[Acetone] [µmol cm^{-2}]	[Carboxylate] [µmol cm^{-2}]	Ac/Ca[a]	Acetone selectivity %[b]
Ti-1	0	–	–	–	–
Ti-20	0.26	0.02	0.01	1.48	–
Ti-40	2.23	0.17	0.1	1.74	63
Ti-60	10.64	0.73	0.67	1.09	77

[a] After 100 minutes. [b] After reaching same product amount, that is, 0.23 µmol cm^{-2}.

indeed remarkable that a surface selectivity in the range of 50–60% can be achieved with the TUD-1 catalysts. Apparently, the physical constraints imposed by the TUD-1 matrix—constraints on anatase particle morphology and perhaps adsorbate mobility—can bias the photocatalytic reaction toward the desired partially oxidized products. Indeed, the average smaller particle size and pore diameter determined for the Ti-60 catalyst compared to the Ti-40 sample is in agreement with this hypothesis, in view of the higher selectivity obtained with the former system. It should also be mentioned that the present study was conducted with 365 nm near–UV light only, rather than with the entire spectrum of deuterium and mercury lamps;[4,5] the use of one wavelength might be beneficial for selective product formation. The effect of the applied wavelength on product selectivity is currently under investigation.

Besides the use of TiO_2 for total oxidation of alkanes in environmental applications, Yoshida and co-workers have reported selective oxidation of propane over SiO_2-supported TiO_2 catalysts in two different publications.[6,7] By comparing the activity data it appears that the same materials were used in both studies, while the reported product distribution differs significantly. In particular, for the catalyst labeled I-TS, studied by Tanaka et al.,[7] a remarkably high selectivity to acetone of 95% was reported, while a selectivity of 57% was reported by Yoshida et al.[6] for the same material under comparable conditions. Regardless of the true performance, in view of the relatively high propane-to-oxygen ratio employed by Yoshida, it appears that Ti incoporated in TUD-1 is a better catalytic system for selective oxidation of hydrocarbons than Ti supported on amorphous silica, especially if one considers the absence of aldehyde formation on the TUD-1 catalysts. The difference in aldehyde selectivity observed for pure TiO_2 phases and Ti-TUD-1 remains an unresolved issue, and needs further investigation.

Finally, in contrast to what is reported for zeolite Y,[21] the primary surface reaction products, acetone and water, could be partially removed by evacuation at room temperature. Figure 13 shows the FTIR spectra for desorption of the products from the TiO_2-TUD-1 surface. Almost 30% of acetone and 10% of water was removed by evacuation after 90 minutes; however, carboxylate species did not show any significant desorption from the catalyst surface. The relatively easy desorption of acetone is a potentially favorable property of TUD-1 in an eventual practical process. Further evaluation of the surface properties of the carboxylates is necessary to design such a process. As a final note, the use of visible-light-active materials or even the reaction without illumination, as discussed by Lefferts,[21] is economically more favorable than the reported UV-driven TiO_2 catalysis. Activity data of visible-light-sensitive Cr-TUD-1 will be reported shortly, indicating that the Cr system is also highly selective in the photooxidation of propane to acetone.

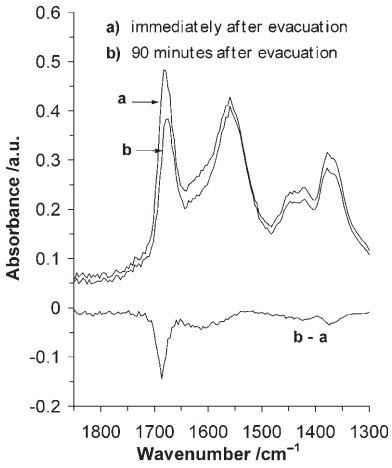

Figure 13. The FTIR spectra recorded during evacuation.

Conclusion

Different active sites can be generated during the synthesis of Ti-containing TUD-1 mesoporous materials. Isolated tetrahedrally coordinated Ti^{4+} species ($Ti-(OSi)_4$) are formed when the Si/Ti ratio is lower than ~2.5. When the fraction of Ti atoms is increased further, nanoparticles of TiO_2 are synthesized inside the pores of TUD-1; the isolated species is also formed. The crystalline phase has been identified as anatase. By using 365 nm near-UV irradiation, which selectively activates the anatase nanoparticles, photooxidation of propane was induced. TiO_2-TUD-1 shows higher selectivity towards acetone than commercial anatase, the sample with a Si/Ti ratio of 1.6 being the most selective. The products could be partially removed from the TiO_2-TUD-1 surface at room temperature by evacuation, which opens up the design for a continuous process.

Experimental Section

Materials synthesis: A series of TiO_2-TUD-1 samples with different Si/Ti ratios (100, 5, 2.3, and 1.6) were synthesized in a one-pot surfactant-free procedure based on a sol–gel technique. Triethanolamine (TEA) functions as a bifunctional template and tetraethyl ammonium hydroxide (TEAOH) as the base.[9–11] In a typical synthesis procedure, using a molar composition of $1\,SiO_2$:$x\,TiO_2$:$0.3\,TEAOH$:$1\,TEA$:$11\,H_2O$, a mixture of triethanolamine (97%, ACROS) and deionized water was added dropwise into a mixture of tetraethylorthosilicate (+98%, ACROS) and titanium(IV) *n*-butoxide (99%, ACROS) while stirring. After stirring for a few minutes, tetraethyl ammonium hydroxide (35%, Aldrich) was added. Finally the mixture was aged for 24 h under atmospheric conditions, dried for 24 h at 371 K, hydrothermally treated at 455 K for 8 h, and calcined at 873 K for 10 h (ramp 1 K min^{-1}).

For comparison, two samples of TiO_2 Hombikat (pure anatase phase; 99% Aldrich) were used to photocatalyze the oxidation of propane. The first sample (Hombikat) was used as obtained. The textured properties of this sample were as follows: the surface area was 337 m^2g^{-1}, pore volume was 0.46 cm^3g^{-1}, and the pore size was 2.2 nm. The second sample (Hombi-600) was calcined before being used at 600°C for 10 h[22] and the textured properties can be summarized as follows: surface area was 51 m^2g^{-1}, pore volume was 0.26 cm^3g^{-1}, and the pore size was 1.4 nm.

Catalyst characterization: Powder XRD patterns were measured on a Philips PW 1840 diffractometer equipped with a graphite monochromator

using $Cu_{K\alpha}$ radiation ($\lambda = 0.1541$ nm). The samples were scanned over a range of 0.1–80° 2θ with steps of 0.02°. Nitrogen adsorption and desorption isotherms were recorded on a QuantaChrome Autosorb-6B at 77 K. The pore size distribution was calculated from the adsorption branch using the Barret–Joyner–Halenda (BJH) model.[23] Samples were previously evacuated at 623 K for 16 h. The Brunauer–Emmett–Teller (BET) method was used to calculate the surface area (S_{BET}) of the samples, while the mesopore volume ($V_{mes}O$) was determined by the t-plot method according to Lippens and de Boer.[24] Instrumental neutron activation analysis (INAA) was used for chemical composition determination (elemental analysis), which was performed at the Interfaculty Reactor Institute (IRI), Delft. The "Hoger Onderwijs Reactor" nuclear reactor, with a thermal power of 2 MW and maximum neutron flux of 10^{17} neutrons $s^{-1} cm^{-2}$, was used as a source of neutrons and the gamma spectrometer was equipped with a germanium semiconductor as the detector. This method can be applied to solid samples and was used because of difficulties encountered when dissolving the samples. The method proceeded in three steps: irradiation of the elements with neutrons in the nuclear reactor, followed by a period of decay, and finally measurement of the radioactivity resulting from irradiation. The energy of the radiation and the half-life period of the radioactivity enabled a highly accurate quantitative analysis.[25] ^{29}Si MAS NMR experiments were performed with a magnetic field of 9.4 T on a Varian VXR-400 S spectrometer operating at 104.2 MHz with pulse width of 3.2 ms. Zirconia rotors (4 mm) were used with a spinning speed of 8 kHz. Chemical shifts were measured with respect to tetramethylsilane (TMS) as an external standard at $\delta = 0$ ppm. 1000 scans were collected using a sweep width of 20000 Hz and an acquisition delay of 20 s. UV-visible spectra were collected at ambient temperature on a CaryWin 300 spectrometer using $BaSO_4$ as a reference. Samples were ground carefully, heated overnight at 180 °C, and then scanned from 190–800 nm. The UV-visible absorption data were converted to Kubelka–Munk units. The laser Raman spectra were obtained by using a Renishaw Raman imaging microscope, system 2000. The green ($\lambda = 514$ nm) polarized radiation of an argon-ion laser beam of 20 mW was used for excitation. A Leica DMLM optical microscope with a Leica PL floutar L500/5 objective lens was used to focus the beam on the sample. The Ramascope was calibrated using a silicon wafer. Samples were dehydrated in situ in an airflow of 100 mL min^{-1}, by using a temperature programmed heated cell (Linkam TS1500). Spectra were collected in the range 180–1600 cm^{-1}. HR-TEM was carried out on a Philips CM30UT electron microscope with a field-emission gun, operated at 300 kV, as the source of electrons. Samples were mounted on a copper-supported carbon polymer grid by placing a few droplets of a suspension of ground sample in ethanol on the grid, followed by drying under ambient conditions. EDX elemental analysis was performed on a LINK EDX system.

Propane photooxidation: Near-UV light was obtained from a 500 W capillary Hg arc (Philips SP500). The intense Hg emission at 365 nm was isolated by means of a monochromator and glass filters, resulting in a bandwidth of approximately 15 nm. Output was measured with a thermopile power meter (Scientech 360001).

Thin wafers of TiO_2-TUD-1 weighing approximately 15 mg were formed at 3 tons cm^{-2} on an automatic press (SPECTA). These were mounted on a copper sample holder that incorporated a resistive heating element and type-K thermocouples. The holder, in turn, was mounted in the optical tail of a stainless steel high-vacuum system (base pressure 6×10^{-8} mbar). The tail was positioned in the sample bay of a purged FTIR spectrophotometer (Bio-Rad 176C). All spectra were averaged over 200 scans at 8 cm^{-1} resolution. By using CaF_2 windows and protecting the detector with a germanium plate, FTIR spectra could be obtained during UV irradiation. The optical layout is illustrated in Figure 14.

All samples were activated by heating under high vacuum to 500 °C (ramp 15 K min^{-1}). 500 °C was maintained for 30 minutes, during which time changes in the IR spectrum—primarily due to the desorption of water—ceased. After cooling to 25 °C, the vacuum chamber was loaded with 2.75 mbar propane and 400 mbar molecular oxygen (this propane/oxygen 1:140 ratio was used for all experiments). These molar quantities are large compared with the amount of adsorbed photochemical products. Thus, the reactions occurred with a large excess of gas-phase reagents at effectively constant concentration. Finally, we note that the absorption of UV light caused an observable heating of the sample wafers. This heating was greater under high vacuum than with the reagent gases present. Evidently the principal heat-loss mechanism under reaction conditions was not lateral thermal diffusion to the copper sample holder, but rather contact with the background gas. A temperature-dependent shift of the O–Si–O absorption intrinsic to TUD-1 was calibrated against resistive heating of the entire sample holder under high vacuum. Using these shifts as an in-situ temperature gauge, the radiative heating effect was found to be less than 20 K.

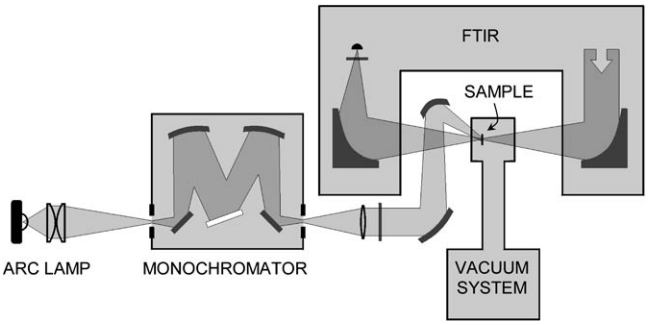

Figure 14. Schematic optical layout for photocatalytic evaluation.

IR absorption spectroscopy : Distribution of the photochemical reaction products is not expected to be uniform within the sample wafer. As such pressed powders absorb and scatter visible light strongly, there will be a gradient of radiation intensity and hence reaction rate, as a function of depth into the sample (parallel to the direction of the infrared beam). The products may or may not redistribute by diffusion. On the other hand, the UV-light image was diffuse and larger than the IR focus, so that the photochemical products were uniformly distributed in the direction transverse to the infrared beam. Under these circumstances a suitable instrumental measure of product concentration is the 2D "column density" in the transverse direction, or molecules cm^{-2}. For linear-absorption measurements it is immaterial how a given number of molecules are distributed in the longitudinal direction. Therefore the Beer–Lambert law may be written as Equation 1, in which I_0 and I are the incident and transmitted light intensity as a function of frequency ν, A is the absorbance, C is the column density (molecules cm^{-2}), and σ is the molecular absorption cross section (cm^2 molecule^{-1}).

$$\ln[I_o(\nu)/I(\nu)] = 2.303\,A(\nu) = C\sigma(\nu) \quad (1)$$

Integrating over frequency gives Equation 2, in which $\tilde{A}$ is the integrated absorbance (band area) and $\tilde{\sigma}$ is the integrated molecular cross section (cm per molecule)

$$\tilde{A} = C\tilde{\sigma}/2.303 \quad (2)$$

The latter is proportional to the transition dipole moment, and so forth. By systematic dosing, we measured $\tilde{\sigma} = 3.24 \times 10^{-17}$ cm per molecule for the C=O stretch of acetone adsorbed to TUD-1. For carboxylate species we used a value typical of adsorbed formate and acetate ions: $\tilde{\sigma} = 4.7 \times 10^{-17}$ cm per molecule.[26]

As the IR spectra of the products overlap, it was necessary to separate these by deconvolution. Good fits could be obtained in the region of interest (1520–1720 cm^{-1}) by the sum of three Gaussian bands and a linear baseline, as shown in Figure 15. With the center frequency of the water band fixed at 1635 cm^{-1}, the other frequencies, widths, and amplitudes were optimized by a nonlinear least-squares fitting procedure. It is the areas of these component Gaussian bands that were used to calculate the

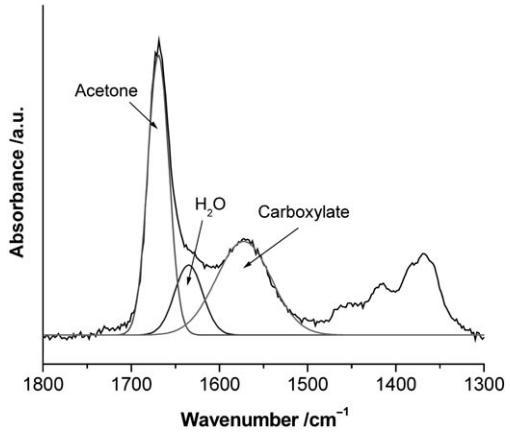

Figure 15. FTIR spectra of adsorped species and their deconvolution.

column density (C) of the adsorbed species. The yield of acetone and carboxylates can then be computed using the component band areas and Equation (2).

Acknowledgements

This work was financially supported by STW. Thanks to Dr. Z. Shan for supervising the synthesis, Dr. P. Kooyman for HR-TEM measurements, Dr. P. Du for TiO_2 anatase samples, and Dr. J. Groen for N_2 sorption measurements. Dr. H. Frei is gratefully acknowledged for fruitful discussions. M.S.H. thanks the Egyptian Government, Ministry of Higher Education for his personal fellowship.

[1] P. Pichat, J.-M. Herrmann, J. Disdier, M.-N. Mozzanega, *J. Phys. Chem.* **1979**, *83*, 3122–3126.
[2] L. V. Lyashenko, Y. B. Gorokhovatskii, V. I. Stepanenko, F. A. Yampolskaya, *React. Kinet. Catal. Lett.* **1979**, *10*, 13–17.
[3] K. Wada, K. Yoshida, T. Takatani, Y. Watanabe, *Appl. Catal. A* **1993**, *99*, 21–36.
[4] C. T. Brigden, S. Poulston, M. V. Twigg, A. P. Walker, A. J. J. Wilkins, *Appl. Catal. B* **2001**, *32*, 63–71.
[5] A. Haeger, O. Kleinschmidt, D. Hesse, *Chem. Eng. Technol.* **2004**, *27*, 1019–1026.
[6] S. Yoshida, S. Takenaka, T. Tanaka, H. Hirano, H. Hayashi, *Stud. Surf. Sci. Catal.* **1996**, *101*, 871–880.
[7] T. Tanaka, K. Teramura, T. Yamamoto, S. Takenaka, S. Yoshida and T. Funabiki, *J. Photochem. Photobiol. A* **2002**, *148*, 277–281.
[8] H. Yoshida, *Curr. Opin. Solid State Mater. Sci.* **2003**, *7*, 435–442.
[9] J. C. Jansen, Z. Shan, L. Marchese, W. Zhou, N. Puil, T. Maschmeyer, *Chem. Commun.* **2001**, 713–714.
[10] Z. Shan, E. Gianotti, J. C. Jansen, J. A. Peters, L. Marchese, T. Maschmeyer, *Chem. Eur. J.* **2001**, *7*, 1437–1443.
[11] Z. Shan, J. C. Jansen, L. Marchese, T. Maschmeyer, *Microporous Mesoporous Mater.* **2001**, *48*, 181–187.
[12] M. Stocker, *Stud. Surf. Sci. Catal.* **1994**, *85*, 429–507.
[13] K. J. MacKenzie, M. E. Smith in *Multinuclear Solid-State NMR of Inorganic Materials*, Pregamon, Oxford, **2002**, pp. 201–268.
[14] W. A. Carvalho, P. B. Varaldo, M. Wallau, U. Schuchardt, *Zeolite* **1997**, *18*, 408–416.
[15] K. Sing, D. Everett, R. Haul, L. Moscou, R. Pierotti, J. Rouquerol, T. Siemieniewska, *Pure Appl. Chem.* **1985**, *57*, 603–619.
[16] S. Klein, B. M. Weckhuysen, J. A. Martens, W. F. Maier, P. A. Jacobs, *J. Catal.* **1996**, *163*, 489–491.
[17] G. Petrini, A. Cesana, G. De Alberti, F. Genoni, P. Rofia, *Stud. Surf. Sci. Catal.* **1991**, *68*, 761–766.
[18] a) L. Miao, P. Jin, K. Kaneko, S. Tanemura, P*rocedings of 8th International conference on electronic materials (IUMRS-ICEM)* **2002**, 944–963; b) L. Miao, S. Tanemura, Y. Kondo, M. Iwata, S. Toh, K. Kaneko, *Appl. Surf. Sci.* **2004**, *238*, 125–131; c) H. T. Nguyen, L. Miao, S. Tanemura, M. Tanemura, S. Toh, K. Kaneko, M. Kawasaki, *J. Cryst. Growth* **2004**, *271*, 245–251.
[19] A. A. Davydov, *Infrared Spectroscopy of Adsorbed Species on the Surface of Transition Metal Oxides*, Wiley, Chichester, **1990**, p. 148.
[20] G. Mul, A. Zwijnenburg, B. van der Linden, M. Makkee, J. A. Moulijn, *J. Catal.* **2001**, *201*, 128–137.
[21] J. Xu, B. L. Mojet, J. G. van Ommen, L. Lefferts, *J. Phys. Chem. B* **2004**, *108*, 218–223.
[22] P. Du, G. Mul, J. A. Moulijn, unpublished results.
[23] E. P. Barret, L. G. Joyner, P. H. Halenda, *J. Am. Chem. Soc.* **1951**, *73*, 373–380.
[24] B. C. Lippens, J. de Boer, *J. Catal.* **1965**, *4*, 319–323.
[25] F. Boynton in *Handbook on the Physics and Chemistry of Rare Earths, Vol. 4* (Eds.: K. Gschneidner, L. Eyring), North-Holland, Amsterdam, **1979**, pp. 457–470.
[26] V. A. Matyshak, O. V. Krylov, *Kintec. Catal.* **2002**, *43*, 391–407.

Received: June 7, 2005
Published online: September 21, 2005

